IN-SILICO DESIGN OF AN ALL-ARMCHAIR GRAPHENE NANORIBBON FIELD EFFECT TRANSISTOR SENSOR FOR THE INDIRECT DETECTION OF STARCH

Isabella López Cifuentes *

*Pontificia Universidad Javeriana Cali
lopezcifu.isabella@gmail.com

ABSTRACT

Starch plays a fundamental role in plants, being an essential molecule to understand their energy transport and storage. Therefore, continuous monitoring of the intracellular synthesis of starch is critical for understanding energy pathways and metabolic regulation in plants. This article highlights the importance of real-time measurement of ultra-low concentration of this metabolite, to detect and manage stress-induced events in plants. Thus, we present the in-silico design of an all-armchair graphene nanoribbon field-effect transistor (GNRFET) device for the detection of ultra-low concentration (pM-nM) amylose. Starch molecules are composed primarily of two glucose polymers: amylopectin and amylose, the latter presenting a linear structure desired for its simplicity and smaller size. We use a self-assembled monolayer (SAM) of a pyrene moiety, 3-[4-(pyren-1-yl)butanamido]phenylboronic acid (PBPBA) adsorbed on the channel, to functionalize the graphene surface. Then covalent binding of the target molecule to the end with phenylboronic acid provides mechanical, chemical, and electronic signal sensing stability. Furthermore, we screened GNRFET configurations with different widths, to control bandgap in the channel, lengths to ensure tunneling transport across the semiconducting junction, and a back-gated channel to optimize electronic transport and switching properties of the device. We demonstrate the channel SAM of PBPBA functionalization improves the signal-to-noise-ratio (SNR) of the device, and estimate its limit of detection (LOD) to be $7.123/n \times 10^{-}2mol/L$ (for a symmetric 2D array configuration with n as the number of sensor units per array dimension). The devices offers an output current sensitivity of $100 - 300nA$, at low gate voltages ($V_G = 1.2V$) and drain-to-source voltage $V_{DS} = 0.6V - 0.8V$, for the detection of 1-2 amylose trimers. Therefore we obtained a low-power all-armchair GNR-FET sensor with SAM PBPBA ligands in the channel that provides a real-time and high throughput solution for sensing amylose (a component of starch)

1. INTRODUCTION

Sucrose and starch are primary metabolites in plants that play a fundamental role in their growth and development [1]. Therefore, continuous monitoring of their intra-cellular synthesis is critical for understanding energy pathways and metabolic regulation in plants. Changes in their levels, correspond to the ultimate biological response to genetic differences or stresses (such as disease or environmental changes). Thus, real-time measurement of these metabolites, capable of relaying the state of these variables without compromising the health of the living organism would be required. Highly efficient and reliable devices able to detect ultra-low concentration of target molecules within cells of a living organism [2].

Accurate and remote sensing is a critical component of precise phenotyping. Conventional tests involve sample taking to subject that sample to a chemical process in a laboratory or if remote, they use temporary labels (such as fluorescence, chemiluminescence, colors, etc) and specific chemical processes. For instance, conventional tests to detect metabolites such as starch comprise iodine tests [3] that use a blue-colored result after a chemical reaction between a part of the starch molecule with iodine molecules; other method consists of solubilizing starch converting it quantitatively to glucose and assaying the glucose enzymatically [4].

However, these methods could be invasive to the plant, they do not necessarily allow to perform sensing on-site or remotely and in some cases do not have low-concentration accuracy, at least at a molecular level. To this end, remote in-vivo and portable ex-vivo sensing of ultra-low concentrations (pM-nM) of significant molecular substances (RNA, DNA, proteins, primary and secondary metabolites, etc) are required. Biomarker sensors offer a potential cost-effective contribution to solve this problem.

To this end, we propose the design and characterization of a label-free Graphene Nanoribbon Field Effect Transistor (GNRFET) with a functionalized channel surface for indirect detection of starch using amylose as analyte.

We use graphene for this application because it is an all-carbon highly-biocompatible material and provides a high-surface area exposed to the target molecules to be sensed. Also it presents metallic or semiconducting behavior depending on the width of nanoribbons, allowing us to design a FET device [5, 6, 7]. We functionalize the semiconducting channel through non-covalent $\pi - \pi$ interactions with pyrene

molecules as bifunctional ligands because of their affinity and self-assembly capabilities on the graphene surface and to reactive capabilities on the other end of the molecule, also it has been extensively used on graphene-based FET sensing devices [5, 8, 9, 10, 11, 12]. Therefore here we use specifically (3-[4-(pyren-1-yl)butanamido]phenyl boronic acid), or PBPBA, taking advantage of the boronic acid affinity to cis-diols in simple sugars [13, 14, 15], obtaining covalent binding and functionalization without affecting the electronic properties of the device and stabilizing the analyte on the channel.

The rest of this article is organized as follows: Section 2 summarizes the computational methods and procedures used in Section 3 to predict the electronic transport properties of the bare channel, the functionalization of it and the consequent sensing capabilities of the device. Section 4 describes the important findings and contributions of this work.

2. METHODS

Quantum mechanical calculations were carried out using Density Functional Theory (DFT) [16] as implemented in QuantumATK package [17][18]. Here, the Kohn–Sham Hamiltonian is expanded into a numerical Linear Combination of Atomic Orbitals (LCAO), Quantum ATK comes with pre-built basis sets of orbitals that represent each chemical element for different pseudopotentials. For the exchange-correlation parameters, we used Generalized Gradient Approximation (GGA) Perdew-Burkey-Ernzenhof (PBE)[19] pseudopotentials Fritz-Haber Institute (FHI) [20] code with Double Zeta Polarized (DZP) basis sets. All DFT calculations included London dispersion corrections (Van der Waals corrections important for the interaction between the graphene and the pyrene base), at the Grimme D3 level[21].

Before any binding energy or transport calculation were performed, all structures simulated were minimized using LBFGS [22] method (with DFT) as implemented in QuantumATK package to a convergence max forces criteria to $0.05eV/\text{Å}$. Also, self-consistent iteration was enabled, using the Pulay mixing scheme (PulayMixing Algorithm [23]) to obtain the best guess for the next input (to a hamiltonian variable). Energy convergence criteria for minimization was $1e-5$ and a damping factor of 0.1. In the case of transport calculations, energy tolerance was $5e-5$, and the damping factor we varied (using 0.1 or 0.05) to reach convergence in some voltages.

For device electronic transport calculations, we used Density Functional based Tight Binding (DFTB)[24] Slater Koster method with Magsil-1-1 [25] parameter set. These are coupled to the non-equilibrium Green's Functions (NEGF) machinery [26], as implemented in Quantum ATK [18]. A Multigrid Poisson solver with a Periodic boundary condition in A and B direction and a Dirichlet boundary condition in the C transport direction was used. For numerical accuracy parameters, we used a Monkhorst-Pack grid with 101 k-points in the C direction (transport direction). The self-consistent energy calculation for a device (with electrodes) is first performed to obtain the Hamiltonian for each of the electrodes under periodic boundary conditions. Then the self-consistent calculation for the central region is performed with open boundary conditions using the self-energies calculated from each electrode. Electronic transport calculations did not include the effect of a solvent (explicit or implicit) different than vacuum.

Energy minimization simulations were also performed using molecular mechanics in LAMMPS [27] to consequently calculate binding energies. Hence, conjugate gradient method was used to minimize the structure geometry until a $1e-6$ RMS force or energy difference was reached. To this end, we used Reactive Force Field (ReaxFF) optimized by our group, based on a REAXFF for DNA [28] but optimized for Boron-Carbon and Boron-Oxygen interactions.

Molecular Dynamics (MD) calculations were carried out in LAMMPS, using the aforementioned ReaxFF along with the charge equilibration method (Qeq) [29], in parallel high-performance computer nodes. All structures were prepared in vacuum using Quantum ATK molecule editor and solvated explicitly, using Packmol package [30], with water molecules to a density of 1g/cc and Potassium (K) counterions to achieve a net-neutral system charge since we used the tetrahedral sp^3 form of PBPBA. We minimized structure geometries a conjugate gradient method to an RMS force or energy difference of $1e-7$ following a temperature equilibration at $300K$ and after a ramp to $350K$ performing time integration on a Nose-Hoover thermostat [31]. We used an NVT canonical ensemble (fixed temperature) over 1 or 2 nanoseconds with a timestep of 0.5 femtoseconds and a damping factor of 50 femtoseconds.

3. RESULTS AND DISCUSSION

3.1. Bare device design and characterization

The architecture of the FET transistor consists of a single 11-10-11 all-armchair graphene nanoribbon (ac-GNR), which corresponds to a $W_E = 11atoms \simeq 1.2nm$ and $W_C = 10atoms \simeq 1.1nm$ for electrodes and channel widths respectively (without hydrogen passivation). Soecifically, nanoribbons of 11 and 10 atoms of carbon wide were used as electrodes and channels, because they present a near-metallic behavior with a bandgap of $0.03eV$ and a semiconducting behavior with a bandgap of $0.9108eV$, respectively.

The channel length is $L_C \simeq 6nm$ and each electrode length showed in Figure 1 is at $L_E = 0.85nm$ with an extension of the same size (for simulation purposes); for practical implementations, the electrodes could be longer and wider, and this would not affect device performance. We used a metallic contact as back gate and a dielectric layer as shown

in Figure 1a which is 3.52Å wide with a dielectric constant of $4.0\epsilon_0$ corresponding to silicon dioxide (SiO_2) (where $\epsilon_0 = 8.854 \times 10^{-12}$ and corresponds to vacuum permittivity).

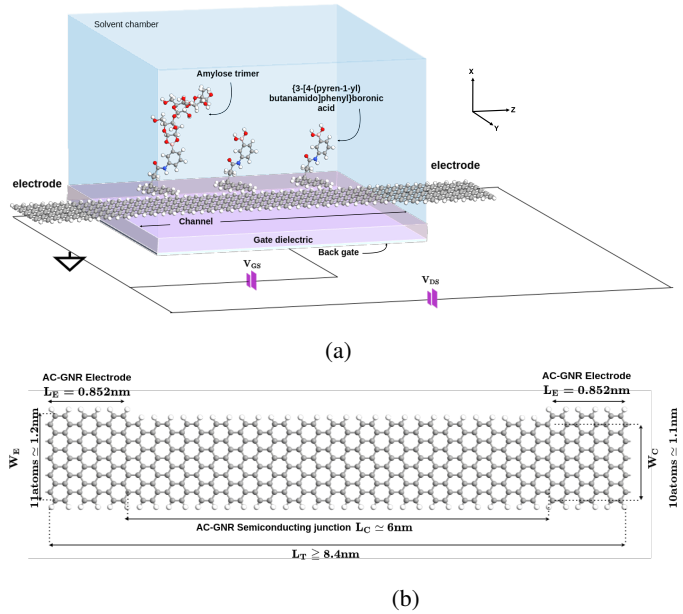

(a)

(b)

Fig. 1: (A) The gnrFET sensor with solvent box in isomeric view with 3 PBPBA Self Assembly Monolayer (SAM) molecules on the channel and 1 bound trimer amylose molecule. A metallic back-gate and under the semiconducting junction a gate oxide separating region. (B) Top view of a bare optimized gnrFETs geometry and dimensions

Analyzing the electronic transport properties of the device, the 11-10-11 configuration presents high conductance capability as depicts Figure 2a. Also the device in general presents low-temperature dependency in the red-shadowed zone (Figure 2a), except for $V_{GS} = 0.5V, -0.5V$. Taking into account that for gate voltages corresponding to $V_G > 0.5V \quad \& \quad VG < -0.5V$ we obtained the highest conductance values along with tunneling transport, we use these voltages later to analyze the sensing response of the device, since we expect that changes in conductance might be induced only by the presence of analytes and not by temperature changes.

3.2. Bifunctionalization with 3-[4-(pyren-1-yl)butanamido] phenylboronic acid

Structurally, starch granules consist of two glucose chains joined by α-1-4 glycosidic bonds are composed of two glucose polymers: amylopectin and amylose. Amylopectin is a highly branched glucose polymer and makes around 65 to 90 % of starch granules, while amylose is considerably smaller and lightly branched. Amylose's glucose chain length varies depending on the plant variety, maturity, etc, so we fixed length to 3 glucose monomers (amylose trimmer) and assume binding takes place on one end of the chain for simplification. For a ligand, we use (3-[4-(pyren-1-yl)butanamido] phenylboronic acid) or PBPBA, as Tlili et al. [12] use in their sensor to selectively detect simple sugars and stabilize the target molecule for detection.

Using DFT and REAXFF, we performed geometry minimization of each of the parts and thereafter compute energies as shown in Table in1.

	DZP (DFT)	ReaxFF
$\mathbf{E_{bind}}$	-18.551 kcal/mol	-19.114 kcal/mol
$\mathbf{E_{physisorption}}$	-49.65 kcal/mol	-37.29 kcal/mol

Table 1: Binding energies for amylose molecule and PBPBA in Sp^3 hybridization, and physisorption energies for bound amylose and PBPBA, on a graphene nanoribbon

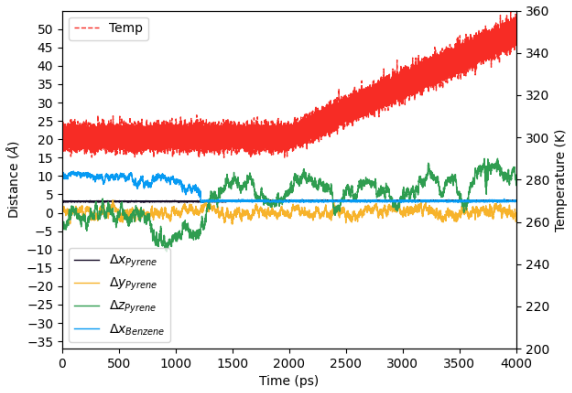

Fig. 3: (A) Difference in x (black), y (yellow) and z (green) coordinates between acGNR's semiconducting junction part and pyrene basal plane; also difference in x (blue) between the benzene group in the PBPBA and the GNR, and red dots correspond to temperature

The binding and physisorption between PBPBA and the analyte and pyrene and GNRs are confirmed, as experimental [12, 9, 11] and other in-silico works [5, 32] have proven. As Table 1 indicates, there is good physisorption energy, indicating that the PBPBA is attracted to the acGNR through strong interactions that will provide stabilization to the amylose on the FET channel. ReaxFF calculations are also consistent with quantum mechanics, which confirms the accuracy of the force field used in MD simulations.

In Figure 3 we confirmed thermodynamic stability of the analyte, where the position of the pyrene base (with the PBPBA and amylose linked) in the x-direction varies between 3.62Å and 2.89Å, maintaining that range even when the temperature increases from 300K to 350K. Besides, during the thermodynamic equilibrium at 300K the benzene group in

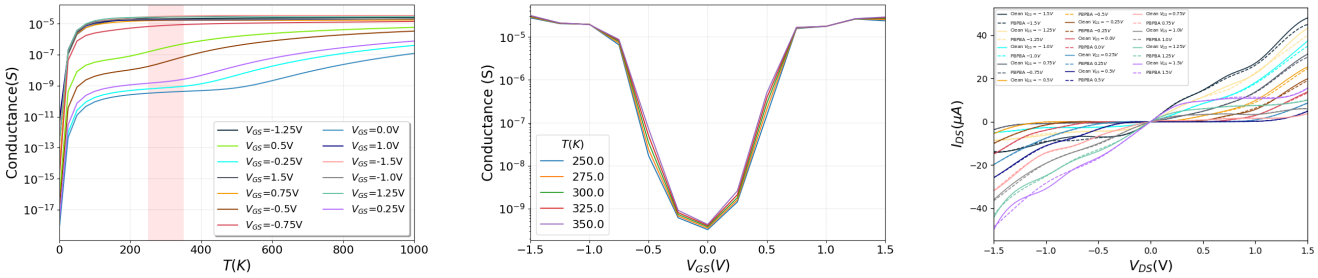

(a) (b) (c)

Fig. 2: (a) Conductance vs Temperature in electrodes, (b) Conductance vs gate voltage for 11-10-11 acGNR nanoribbon configuration and (c) IV characteristics plot comparing the bare and functionalized channel with three PBPBA in a SAM

the PBPBA also ends physisorped on the graphene's surface and remains in that form, meaning further stabilization by reducing the mobility of the pyrene end and consequently, the analyte.

3.3. Device detection of amylose trimers

.

Figure 2c confirms that the presence of pyrene ligands on the channel does not alter the transport properties of the bare transistor, especially for $-1.0V < V_{DS} < 1.0V$. This is a critical feature since it allows us to detect and distinguish the sensing signal of an amylose molecule bound to the PBPBA while the pyrene itself does not have a significant effect on the electronic response of the transistor.

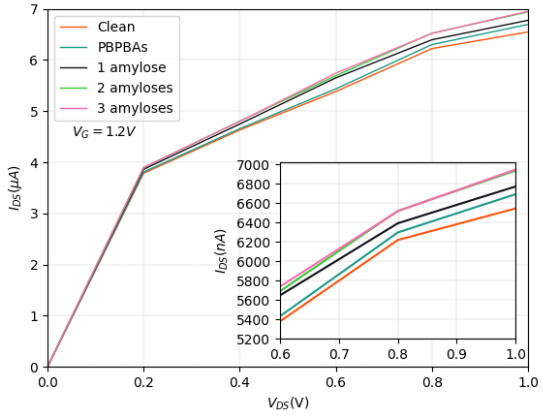

Fig. 4: IV characteristics of 11-10-11 device for PBPBA SAM with no linked, one and two amylose molecules, and three for $V_{GS} = 1.2V$ compared to the clean reference performance (orange line). Inset depicts plot in nano amperes

Resulting IV characteristics, after fixing V_{GS}, show how linked amyloses have an effect on the transport through the channel. For gate voltage $1.2V$, inset in Figure 4 depicts a difference range of $100 - 300nA$ for $V_{DS} = 0.6V$ to $1.0V$ between the functionalized transistor and 1 bound amylose, and $\sim 100nA - 150nA$ difference for the same range in V_{DS}, enough to distinguish 1 from 2 amyloses. Amylose molecules that are bound to the SAM layer could be presenting an electrostatic gating effect on the channel, (acting as a second gate) increasing the available density of states in the channel, however for 3 amyloses it appears that the device reaches saturation thus its current signal is hard to distinguish from the 2 amyloses signal. Thus, our device offers single amylose detection (for 1-2 molecules) bound to the SAM layer.

4. CONCLUSIONS

We demonstrated an in-silico Field-effect transistor (FET) design with electrodes (source, drain) and semiconducting channel junctions made out only by armchair graphene nanoribbons with a back-gate, obtaining a minimal footprint layout ($11.76\ nm^2$) with high current capabilities and low dependency of temperature in conductivity. The usage of a phenyl boronic acid molecule that selectively binds to diols chemical groups in amylose trimmers allowed to functionalize a pyrene-based ligand (PBPBA) that also presents affinity to graphene, thus exhibiting strong physisorption capabilities to its surface. On that account, we obtained a general functionalization of the GNR, that does not perturb the intrinsic electronic response of the device and allowing any change in transport to be a direct effect of an amylose presence. Additionally, we confirmed that the pyrene-moiety ligands remain absorbed on the graphene surface and bound to the amylose, even under physiological temperature conditions. Therefore providing physical, chemical and mechanical stabilization of the amylose trimer on the GNR, reducing its mobility and consequently noise in the electronic output signal.

Furthermore we achieved detection of single amylose-trimer molecules, for 1-2 molecules with differences in current between $100 - 300nA$ at relatively low voltages

$V_G = 1.2V$ and $V_{DS} = 0.6 - 0.8V$, with a LOD of 7,123 $\times 10^{-2} mol/L$ for a single transistor. This provides the basic node for a potential 2D nano-array device architecture, e.g. 1000x1000 or $n \times n$ transistors with LOD of 71.23 $\mu M/L$ or 7,123/n $\times 10^{-2} mol/L$ respectively (assuming a node footprint of $11.76nm^2$ and a volumetric height of $3.5nm$, for a total of $41.26nm^3$ per detection node). Therefore, this proof of concept could be projected to make more complex sensors based on a basic design that provides real-time, high throughput solution to sensing short-length polysaccarides like amylose trimmers. The remaining question relies on assuring selectivity of the sensor and differentiation of amylose and other simple sugars or polysaccarides.

ACKNOWLEDGMENTS: This work was partially funded by the "OMICAS program: Optimización Multiescala Insilico de Cultivos Agrícolas Sostenibles (Infraestructura y validación en Arroz y Caña de Azúcar)" Scientific Ecosystem belonging to the Colombia Científica Program, sponsored by The World Bank, The Ministry of Science, Technology and Innovation (MINCIENCIAS), ICETEX, the Colombian Ministry of Education and the Colombian Ministry of Commerce, Industry and Turism, under GRANT ID: FP44842-217-2018, OMICAS Award ID: 792-61187.

5. REFERENCES

[1] L. M. Solarte, R. D. Escandon, D. Hermith, P. M. Hernandez-Acosta, E. Tamura, L. E. Tobon, H. D. Benitez-Restrepo, and A. Jaramillo-Botero, "Phenosense midterm report," Pontificia Universidad Javeriana Cali and California Institute of Technology and International Center for Tropical Agriculture (CIAT), Tech. Rep., February 2017.

[2] S. Mohanty, "Biosensors : A Tutorial Review Biosensors : A Tutorial Review," *IEEE Potentials*, vol. 25, no. APRIL 2006, pp. 35–40, 2015.

[3] R. Smith, E. Lougheed, E. Franklin, and I. McMillan, "The starch iodine test for determining stage of maturation in apples," *Canadian Journal of Plant Science*, vol. 59, no. 3, pp. 725–735, 1979.

[4] A. M. Smith and S. C. Zeeman, "Quantification of starch in plant tissues," *Nature protocols*, vol. 1, no. 3, pp. 1342–1345, 2006.

[5] A. Jaramillo-Botero and J. M. Marmolejo-Tejada, "All-armchair graphene nanoribbon field-effect uridine diphosphate glucose sensor: First-principles in-silico design and characterization," *IEEE Sensors Journal*, vol. 19, no. 11, pp. 3975–3983, 2019.

[6] J. H. Warner, F. Schaffel, M. Rummeli, and A. Bachmatiuk, *Graphene: Fundamentals and emergent applications*. Newnes, 2012, ch. 2.5, pp. 33–49.

[7] L. Yang, C.-H. Park, Y.-W. Son, M. L. Cohen, and S. G. Louie, "Quasiparticle energies and band gaps in graphene nanoribbons," *Physical Review Letters*, vol. 99, no. 18, p. 186801, 2007.

[8] V. Georgakilas, M. Otyepka, A. B. Bourlinos, V. Chandra, N. Kim, K. C. Kemp, P. Hobza, R. Zboril, and K. S. Kim, "Functionalization of graphene: covalent and non-covalent approaches, derivatives and applications," *Chemical reviews*, vol. 112, no. 11, pp. 6156–6214, 2012.

[9] D. K. H. Tsang, "Chemically functionalised graphene biosensor for the label-free sensing of exosomes," Ph.D. dissertation, Imperial College London, 2019.

[10] C. Haslam, S. Damiati, T. Whitley, P. Davey, E. Ifeachor, and S. A. Awan, "Label-free sensors based on graphene field-effect transistors for the detection of human chorionic gonadotropin cancer risk biomarker," *Diagnostics*, vol. 8, no. 1, p. 5, 2018.

[11] G. Seo, G. Lee, M. J. Kim, S.-H. Baek, M. Choi, K. B. Ku, C.-S. Lee, S. Jun, D. Park, H. G. Kim *et al.*, "Rapid detection of covid-19 causative virus (sars-cov-2) in human nasopharyngeal swab specimens using field-effect transistor-based biosensor," *ACS nano*, vol. 14, no. 4, pp. 5135–5142, 2020.

[12] C. Tlili, S. Badhulika, T.-T. Tran, I. Lee, and A. Mulchandani, "Affinity chemiresistor sensor for sugars," *Talanta*, vol. 128, pp. 473–479, 2014.

[13] K. T. Kim, J. J. Cornelissen, R. J. Nolte, and J. C. v. Hest, "Polymeric monosaccharide receptors responsive at neutral ph," *Journal of the American Chemical Society*, vol. 131, no. 39, pp. 13 908–13 909, 2009.

[14] J. Yan, G. Springsteen, S. Deeter, and B. Wang, "The relationship among pka, ph, and binding constants in the interactions between boronic acids and diols—it is not as simple as it appears," *Tetrahedron*, vol. 60, no. 49, pp. 11 205–11 209, 2004.

[15] W. L. Brooks, C. C. Deng, and B. S. Sumerlin, "Structure–reactivity relationships in boronic acid–diol complexation," *ACS omega*, vol. 3, no. 12, pp. 17 863–17 870, 2018.

[16] S. Smidstrup, D. Stradi, J. Wellendorff, P. A. Khomyakov, U. G. Vej-Hansen, M.-E. Lee, T. Ghosh, E. Jónsson, H. Jónsson, and K. Stokbro, "First-principles green's-function method for surface calculations: A pseudopotential localized basis set approach," *Physical Review B*, vol. 96, no. 19, p. 195309, 2017.

[17] S. Smidstrup, T. Markussen, P. Vancraeyveld, J. Wellendorff, J. Schneider, T. Gunst, B. Verstichel, D. Stradi,

P. A. Khomyakov, U. G. Vej-Hansen *et al.*, "Quantumatk: An integrated platform of electronic and atomic-scale modelling tools," *J. Phys: Condens. Matter*, vol. 32, p. 015901, 2020.

[18] 2020, quantumATK version Q-2020.09, Synopsys QuantumATK (www.synopsys.com/silicon/quantumatk.html).

[19] J. P. Perdew, K. Burke, and M. Ernzerhof, "Generalized gradient approximation made simple," *Physical review letters*, vol. 77, no. 18, p. 3865, 1996.

[20] V. Blum, R. Gehrke, F. Hanke, P. Havu, V. Havu, X. Ren, K. Reuter, and M. Scheffler, "Ab initio molecular simulations with numeric atom-centered orbitals," *Computer Physics Communications*, vol. 180, no. 11, pp. 2175–2196, 2009.

[21] S. Grimme, J. Antony, S. Ehrlich, and H. Krieg, "A consistent and accurate ab initio parametrization of density functional dispersion correction (dft-d) for the 94 elements h-pu," *The Journal of chemical physics*, vol. 132, no. 15, p. 154104, 2010.

[22] D. C. Liu and J. Nocedal, "On the limited memory bfgs method for large scale optimization," *Mathematical programming*, vol. 45, no. 1, pp. 503–528, 1989.

[23] P. Pulay, "Convergence acceleration of iterative sequences. the case of scf iteration," *Chemical Physics Letters*, vol. 73, no. 2, pp. 393–398, 1980.

[24] M. Elstner, D. Porezag, G. Jungnickel, J. Elsner, M. Haugk, T. Frauenheim, S. Suhai, and G. Seifert, "Self-consistent-charge density-functional tight-binding method for simulations of complex materials properties," *Physical Review B*, vol. 58, no. 11, p. 7260, 1998.

[25] J. Frenzel, A. Oliveira, N. Jardillier, T. Heine, and G. Seifert, "Semi-relativistic, self-consistent charge slater-koster tables for density-functional based tight-binding (dftb) for materials science simulations," *Zeolites*, vol. 2, no. 3, p. 7, 2004.

[26] M. Brandbyge, J.-L. Mozos, P. Ordejón, J. Taylor, and K. Stokbro, "Density-functional method for nonequilibrium electron transport," *Physical Review B*, vol. 65, no. 16, p. 165401, 2002.

[27] S. Plimpton, "Fast parallel algorithms for short-range molecular dynamics," *Journal of computational physics*, vol. 117, no. 1, pp. 1–19, 1995.

[28] C. C. W. Verlackt, E. C. Neyts, T. Jacob, D. Fantauzzi, M. Golkaram, Y.-K. Shin, A. C. T. van Duin, and A. Bogaerts, "Atomic-scale insight into the interactions between hydroxyl radicals and DNA in solution using the ReaxFF reactive force field," *New Journal of Physics*, vol. 17, no. 10, p. 103005, oct 2015. [Online]. Available: https://doi.org/10.1088/1367-2630/17/10/103005

[29] H. M. Aktulga, J. C. Fogarty, S. A. Pandit, and A. Y. Grama, "Parallel reactive molecular dynamics: Numerical methods and algorithmic techniques," *Parallel Computing*, vol. 38, pp. 245–259, 2012.

[30] L. Martínez, R. Andrade, E. G. Birgin, and J. M. Martínez, "Packmol: a package for building initial configurations for molecular dynamics simulations," *Journal of computational chemistry*, vol. 30, no. 13, pp. 2157–2164, 2009.

[31] W. Shinoda, M. Shiga, and M. Mikami, "Rapid estimation of elastic constants by molecular dynamics simulation under constant stress," *Physical Review B*, vol. 69, no. 13, p. 134103, 2004.

[32] M. Hinnemo, J. Zhao, P. Ahlberg, C. Hägglund, V. Djurberg, R. H. Scheicher, S.-L. Zhang, and Z.-B. Zhang, "On monolayer formation of pyrenebutyric acid on graphene," *Langmuir*, vol. 33, no. 15, pp. 3588–3593, 2017.